Microwave Measurements for Metal Vessels

Microwave Measurements for Metal Vessels

Livia Cerullo*, Johan Nohlert†, Johan Winges†, Thomas Rylander†,
Tomas McKelvey†, Lubomir Gradinarsky‡, Mats Viberg†, and Staffan Folestad‡

*Department of Signals and systems, Chalmers University of Technology
SE-41296 Göteborg, Sweden, Email: cerullo@chalmers.se
†Department of Signals and systems, Chalmers University of Technology
SE-41296 Göteborg, Sweden
‡AstraZeneca R&D, Pharmaceutical Development, SE-431 83 Mölndal, Sweden

***Abstract*—We present two different measurement techniques intended for closed metal vessels, where the objective is to measure the permittivity inside the metal vessel. This problem is relevant for many applications found in e.g. process industry. The first approach exploits the measurement of resonance frequencies, where the metal vessel is used as a microwave resonator. In the second approach, we let the boundary of the metal vessel be equipped with aperture antennas, where the aperture antennas are implemented in terms of rectangular waveguides. The waveguide apertures loads the cavity significantly and we exploit the scattering matrix parameters for the solution of the inverse problem.**

***Index Terms*—inverse scattering, parameter estimation, eigenvalue problem, scattering matrix**

I. Introduction

Inverse problems arise in many industrial settings [1], where some examples can be found in monitoring of industrial processes [2] and non-destructive testing [3]. To give some examples, we mention the measurement of particulate flow [4] and humidity [5]. Here, we are particularly interested in pharmaceutical processes. The complex nature of pharmaceutical processes makes them difficult to monitor and control, in particular for real-time applications. Conventional measurement techniques are often not sufficiently good, e.g. probes provide mainly local information and they can interfere with the process. Thus, it is of interest to find advanced sensors techniques that can be integrated in the process vessel for in-situ measurements. The well-established electrical capacitance tomography (ECT) has been used to some extent [6]. This technique is fast and low cost but it suffers from relatively low spatial resolution [7].

In this paper, we propose a novel application that exploits two microwave measurement techniques. Microwaves have a number of attractive features: (i) microwaves are non-invasive; (ii) they are non-destructive; (iii) they can provide information about the entire process vessel; and (iv) the contrast with respect to water is high for microwaves. We present a comparative study for two different microwave measurement techniques, where the first one involves a weakly damped vessel and the second one a strongly damped vessel. In the first case, the cavity acts as a microwave resonator and the eigenmodes are exploited to evaluate the dielectric permittivity of the object under test. In the second experiment, we exploit propagating electromagnetic waves for the estimation of the process state. Furthermore, we exploit a new approach based on precomputing responses of the measurement system and store these results in a large database, which is used as a look-up table.

II. Experimental setup

Figure 1 shows a typical process vessel that is exploited in pharmaceutical processes. The process vessel is a closed metal cavity that consists of an upper circular cylindrical part that is connected to a lower conical part. The lower part of the metal cavity hosts a so-called Wurster tube, which is supported by three thin metal struts.

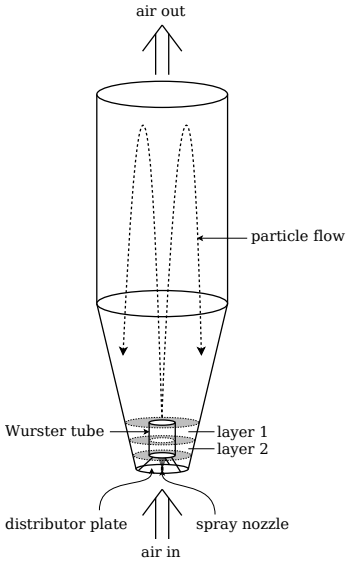

Fig. 1. Process vessel with a Wurster tube supported by three struts. The process vessel is equipped with microwave sensors: (i) one or several magnetic field probes for the upper part of the cavity; and (ii) microwave antennas placed around the circumference of the two annular regions labeled by "layer 1" and "layer 2".

This process vessel is loaded with a batch of a large number of small dielectric granules, which typically fill up the lower part of the vessel such that the supporting struts and a smaller part of the Wurster tube are buried in granules. The bottom

circular surface is referred to as the distributor plate, which is perforated with a large number of small holes. Air that passes through the distributor plate fluidizes the granules such that a fluidized bed is created. A small spray nozzle is located at the center of the distributor plate. The spray nozzle injects an air-liquid mixture into the cavity such that the granules in the immediate vicinity of the nozzle are accelerated through the Wurster tube in an upward motion that creates a fountain above the Wurster tube. The granules in the fountain fall down into the fluidized bed, which completes the circulation of granules inside the process vessel. The air-liquid mixture that is injected through the spray nozzle contains the pharmaceutical active substance in liquidized form, which is deposited on the surface of the granules. As the granules pass through the Wurster tube and the fountain above the Wurster tube, the liquid with the active substance on the surface of the granules dry, which creates a solid coating of active substance on the surface of the granules. After the coating of the granules and other following processing steps are completed, the granules are compressed into pills or packaged in capsules.

The coating process is difficult to control: (i) too rapid coating results in granules that agglomerate and, thus, the fluidized bed collapses and the entire batch is wasted; or (ii) too slow coating yields excessive process times and the liquidized active substance may evaporate before it is deposited on the surface of the granules. Thus, it is of interest to monitor the moisture content inside the process vessel and, in this article, we propose to exploit a combination of microwave sensors that exploit (i) eigenmodes for the upper part of the cavity and (ii) propagating microwaves in the region around the Wurster tube. These measurement techniques are tested in somewhat simplified settings and compared to each other. In particular, we present a computational investigation of a circular array of aperture antennas around the circumference of "layer 1" and "layer 2" in Fig. 1, which can be used to detect bubbles in the fluidized bed.

A. Weakly damped vessel

The usage of weakly damped eigenmodes for the estimation of dielectric properties is tested by means of the metal cavity shown in Fig. 2, which is identical to the cylindrical part of the process vessel shown in Fig. 1. The cavity is equipped with two loop probes soldered to SMA-connectors that are attached to the wall of the cavity, as shown in Fig. 2. A network analyzer is connected to the two probes and we measure the scattering matrix for these two ports.

We exploit the finite element method [8] to solve the eigenvalue problem

$$(\nabla \times \nabla \times -\omega_m^2 \mu_0 \epsilon_0 \epsilon_{\mathrm{r}}) \boldsymbol{E}_m = \boldsymbol{0} \tag{1}$$

with the boundary condition $\hat{\boldsymbol{n}} \times \boldsymbol{E}_m = \boldsymbol{0}$ on the metal surfaces. Given the m-th eigenvalue ω_m together with the corresponding eigenmode $\boldsymbol{E}_m$, we relate the perturbation in the resonance frequency $\delta\omega_m$ to the perturbation in the relative permittivity $\delta\epsilon_{\mathrm{r}}$ by the relation [9]

$$\frac{\delta\omega_m}{\omega_m} = -\frac{\int_V \epsilon_0 \delta\epsilon_{\mathrm{r}} |\boldsymbol{E}_m|^2 dv}{\int_V \epsilon_0 \epsilon_{\mathrm{r}} |\boldsymbol{E}_m|^2 + \mu_0 |\boldsymbol{H}_m|^2 dv}. \tag{2}$$

Fig. 2. Photograph of the finite circular cylinder cavity with its two loop-probes.

Thus, we perform a measurement of the lowest resonance frequencies for (i) an empty cavity and (ii) the cavity with the sample under measurement. Given the relative perturbation $\delta\omega_m/\omega_m$ in the measured frequency for the m-th eigenmode, we exploit Eq. (2) to compute an estimate for the perturbation $\delta\epsilon_{\mathrm{r}}$, where we use the corresponding eigenmode with the electric field $\boldsymbol{E}_m$ and the magnetic field $\boldsymbol{H}_m$ that are computed by means of the eigenvalue problem (1). We combine this procedure for lowest eigenmodes $m = 1, \ldots, M$ and formulate a system of linear equations, which allows us to estimate a few parameters that describe the perturbation in the relative permittivity.

B. Strongly damped vessel

Our second measurement strategy is applied to the fluidized bed and, in particular, we consider "layer 1" and "layer 2" in Fig. 1. Each layer is bounded in the vertical direction by two metal nets, where the metal nets coincide with the gray surfaces in Fig. 1. The metal nets yield an approximate parallel plate waveguide that is operated for the fundamental mode. A number of aperture antennas are uniformly distributed around the circumference of the annular regions referred to as "layer 1" and "layer 2". These antennas are used in both transmitting and receiving mode in order to estimate the distribution of dielectric granules within the layer.

In order to test this type of measurement strategy, we have built a prototype experiment that features six rectangular waveguides (WR-229) that are connected to a measurement region, where the experimental setup are shown in Fig. 3. We place the sample subject to measurement in the region where the waveguides intersect, which is referred to as the measurement region. (This sensor arrangement corresponds to the extreme case where the vessel's vertical wall is completely replaced by aperture antennas.) In Fig. 3, two circular cylinders of plexiglas are placed in the measurement region. Before the measurement is performed, the measurement cavity is covered by a metal lid that completely shields the experiment from the

surrounding environment. Each of the rectangular waveguides is connected to an adapter with a coaxial cable. Further, the coaxial cables are connected to a switch and a network analyzer controls the switch and performs the measurement of the complete scattering matrix in an automatized fashion.

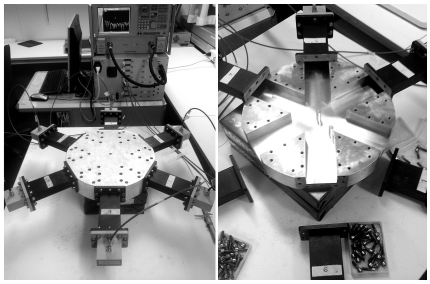

Fig. 3. Photograph of the strongly damped vessel.

We exploit the finite element method [8] to solve the field problem, which can be expressed as

$$\nabla \times (\epsilon^{-1} \nabla \times \boldsymbol{H}) - \omega^2 \mu_0 \boldsymbol{H} = \boldsymbol{0} \tag{3}$$

$$\hat{\boldsymbol{n}} \times (\epsilon^{-1} \nabla \times \boldsymbol{H}) + \gamma^{(p)}\, \hat{\boldsymbol{n}} \times \hat{\boldsymbol{n}} \times \boldsymbol{H} = \boldsymbol{Q}^{(p)} \tag{4}$$

$$\hat{\boldsymbol{n}} \times (\epsilon^{-1} \nabla \times \boldsymbol{H}) = \boldsymbol{0}. \tag{5}$$

Here, we solve Maxwell's equations (3) for the measurement region and a part of the rectangular waveguides. The p-th waveguide port is modeled by the boundary condition (4) with $\gamma^{(p)} = j\omega Z_{10}$, $\boldsymbol{Q}^{(p)} = 2j\omega Z_{10} \hat{\boldsymbol{n}} \times \hat{\boldsymbol{n}} \times \boldsymbol{H}_p^+$, Z_{10} is the wave impedance, $\hat{\boldsymbol{n}}$ is the outward pointing normal and $\boldsymbol{H}_p^+$ is the incident field at port p, i.e., the fundamental waveguide mode TE_{10} [9]. The metal surfaces are modeled as a perfect electric conductor (PEC) by the boundary condition (5).

This model yields a 2D problem for the plexiglas samples shown in Fig. 3, since the 3D parts such as the adapters are located outside the computational domain. Thus, it is possible to perform efficient computations and we exploit this by generating a database for the system response, where the database stores the computed scattering matrix for the system with six ports as a function of frequency. Then, we perform a measurement and solve the inverse problem by a look-up procedure based on the root-mean-square (RMS) deviation between the measured scattering parameters S_{pq}^{M} and the computed result S_{pq}^{C} according to

$$g(\mathbf{a}) = \sqrt{\frac{1}{N^2} \sum_{p=1}^{N} \sum_{q=1}^{N} \frac{1}{f_2 - f_1} \int_{f_1}^{f_2} |S_{pq}^{\mathrm{C}}(f;\mathbf{a}) - S_{pq}^{\mathrm{M}}(f)|^2 df} \tag{6}$$

where $\mathbf{a}$ is a parameter vector with the degrees of freedom that describe the object under measurement. This approach requires massive computations in order to achieve a sufficiently large database that can be used to avoid the problems associated with local minima.

III. Experimental results

Here, we present some initial results for the two experimental setups in a comparative fashion. First, a circular cylindrical plexiglas sample of radius 5.2 mm and length 30.0 mm is measured in the finite circular cylinder cavity shown in Fig. 2. The sample is placed at the center of the bottom plate of the cavity such that its symmetry axis coincides with the symmetry axis of the cavity. Based on the mode TM_{010} with the resonance frequency 918 MHz, which has an electric field maxima at the location of the sample, we estimate the relative permittivity of the sample to be 2.62 ± 0.07. The accuracy of this estimation is limited mainly by (i) the uncertainty in the dimensions of the sample and (ii) the small frequency shift that is introduced as we disassemble and reassemble the top plate of the cavity in order to insert the sample.

Next, we exploit the experiment shown in Fig. 3 to perform measurements on sample configurations, which involve one or several circular cylindrical plexiglas samples of the same type as mentioned above. Here, we present measurement results for three different configurations composed of (i) one cylindrical sample; (ii) three cylindrical samples placed in a packed triangular configuration; and (iii) seven cylindrical samples placed in a packed hexagonal configuration with one cylinder at the center. The three different sample configurations are shown in Fig. 4.

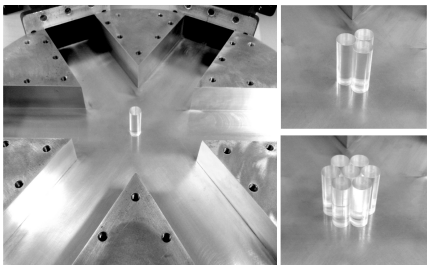

Fig. 4. Sample configurations that consist of one, three and seven circular cylindrical plexiglas samples.

Given the (known) position and geometry for these three test cases, we create a database with a parameterized relative permittivity in the range from 1.5 to 5, where the database stores the system response computed by solving Eqs. (3)-(5). Figure 5 shows the deviation in Eq. (6) between the measured and computed result as a function of the relative permittivity. The minimum occurs at the permittivity value of 2.56 for all the three sample configurations, which demonstrates the consistency and repeatability of this experimental approach. This value is within the permittivity interval 2.62 ± 0.07 that results from the experiment with the cavity resonator. (It should be noted that the resonance frequency for the cavity resonator is located below the frequency band associated with single mode propagation of the WR-229.) We conclude that it is feasible to achieve consistent estimates on the permittivity based on the experimental arrangement shown in Fig. 3.

IV. Computational study for the fluidized bed

In this section, we present a computational study for the fluidized bed. The fluidization process yields an inhomogeneous distribution of granules in the bed region and, in particular,

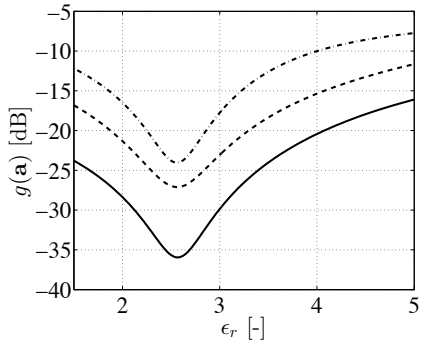

Fig. 5. Usage of database to determine the relative permittivity according to Eq. (6) for three different samples configurations: solid curve – one sample; dashed curve – three sample cylinders placed in a packed triangular configuration; and dash-dotted curve – seven sample cylinders placed in a packed hexagonal configuration with one cylinder at the center.

bubbles of lower or higher granule density may be formed in the fluidized bed. Such bubbles move through the fluidized bed and inhomogeneous material distributions of this type make it more complicated to estimate the effective permittivity in this region.

Here, we propose to exploit three metal nets that are placed horizontally in the region where the fluidized bed is located as shown in Fig. 1: (i) the first net is aligned with the top of the Wurster tube; (ii) the second net is aligned with the mid of the Wurster tube; and (iii) the third net is aligned with the bottom of the Wurster tube. The mask size should be sufficiently large to allow the granules to easily move through the net, such that the fluid dynamical problem is not significantly influenced by the presence of the three nets. However, the mask size is also sufficiently small to provide a decent approximation to a metal surface and, consequently, this yields two layers that are shielded from each other and the other parts of the process vessel. Thus, each layer yields a propagation environment that can be approximated as a parallel plate waveguide and, in combination with sensors, this setup is very similar to the experiment shown in Fig. 3. In the following, we assume that both the geometry and the field solution is approximately two dimensional within the annular region of each layer and, moreover, that the electric field is approximately vertical in Fig. 1.

Thus, we approximate the field problem associated with such a layer by means of a two-dimensional transverse magnetic (TM) problem, which is solved by means of Eqs. (3)-(5). The geometry of "layer 1" allows for six waveguides around the circumference of the circular layer of radius 6.54 cm, as shown in Fig. 6. Here, the outer boundary of the circular layer is shown by the dashed circle and the thick solid curves show metal boundaries. This figure also shows the Wurster tube of radius 2.6 cm at the center of the cavity by means of a thick solid circle. Consequently, the region that is subject to measurement is bounded by $2.6\ \mathrm{cm} < r < 6.54\ \mathrm{cm}$, where r is the radial coordinate in the polar coordinate system associated with Fig. 6. (The interior of the Wurster tube $r < 2.6\ \mathrm{cm}$ is shielded from the aperture antennas and, therefore, this region is not part of the measurement domain.)

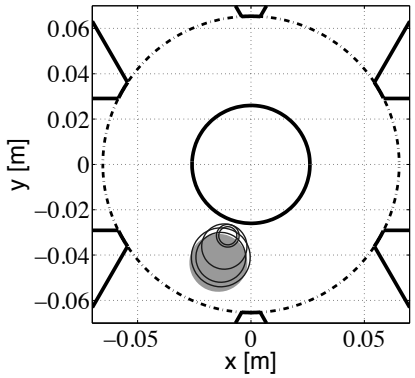

Fig. 6. Geometry and reconstruction for "layer 1": thick solid curves – PEC boundaries; gray circular area – bubble of lower density as compared to the background medium that occupies the remaining portion of the annular region $2.6\ \mathrm{cm} < r < 6.54\ \mathrm{cm}$; and thin solid circles – the five best local optima in the database according to the criterion (6).

We have artificially generated data for $S^{\mathrm{M}}_{pq}(f)$ in Eq. (6) by means of computations for a particular case:

- A circular region, also referred to as an inclusion or a bubble, of radius 12.8 mm is located with its center at $x = -1.44$ cm and $y = -4.34$ cm. The permittivity of the bubble is 3.71 and its conductivity is 0.034 S/m. This region is shown by the shaded area in Fig. 6.
- The remaining part of the fluidized bed, i.e. the background medium, has the permittivity 4.70 and the conductivity 0.056 S/m. (Thus, the background medium is denser than the bubble.)

Next, we exploit a precomputed database with system responses $S^{\mathrm{C}}_{pq}(f;\mathbf{a})$ that features a parameter vector $\mathbf{a}$ with the following parameters:

- Radius of bubbles: 3 mm to 14 mm in steps of 1 mm
- Position of bubbles represented in terms of polar grid with
  - radial coordinates: 32.2 mm, 37.2 mm, 42.2 mm, 47.2 mm, 52.2 mm
  - azimuth coordinates: 30 uniformly spaced grid points for the circumference
- For both the bubbles and the background medium, we use the 60 different combinations of the material parameters (permittivity and conductivity) that are shown in Fig. 7

This yields a database of a large number of different parameter combinations: "layer 1" – 4,968,000 different cases; and "layer 2" – 3,240,000 different cases. (Some parameter combinations from the list above are excluded due to constrains such as that the bubble may not intersect with a PEC boundary.)

The five best local minima in the database, based on the RMS deviation (6) between the measured scattering parameters S^{M}_{pq} and the computed result S^{C}_{pq}, are shown by the thin solid circles in Fig. 6 and the parameter values shown in Tab. I.

Figure 8 and Tab. II show the corresponding results for "layer 2". Note that "layer 2" has a smaller radius of 5.85 cm

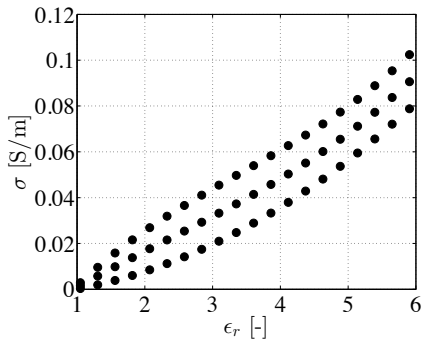

Fig. 7. Combinations of the relative permittivity and the conductivity that are included in the parameter study.

TABLE I
THE FIVE BEST LOCAL MINIMA THAT ARE FOUND IN THE DATABASE FOR LAYER 1, WHERE THESE ARE SORTED IN TERMS OF THE VALUE OF THE DEVIATION EQ.(6) WITH THE SMALLEST VALUE ON THE FIRST ROW.

Inclusion					Background	
r_0 [m]	x [m]	y [m]	ϵ_{r} [-]	σ [S/m]	ϵ_{r} [-]	σ [S/m]
0.013	-0.0133	-0.0410	4.12	0.038	4.63	0.060
0.011	-0.0133	-0.0410	3.86	0.033	4.63	0.060
0.010	-0.0118	-0.0362	3.86	0.033	4.63	0.060
0.005	-0.0102	-0.0315	2.33	0.011	4.63	0.060
0.004	-0.0102	-0.0315	1.31	0.002	4.63	0.060

and, therefore, it is only feasible to fit five aperture antennas around the circumference of "layer 2". Here, we consider the following case:

- A circular region of radius 7.1 mm is located with its center at $x = 3.15$ cm and $y = -2.29$ cm. The permittivity of the bubble is 4.84 and its conductivity is 0.062 S/m. This region is shown by the shaded area in Fig. 8.
- The surrounding part of the fluidized bed, i.e. the background medium, has the permittivity 3.43 and the conductivity 0.038 S/m. (Thus, the background medium is thinner than the circular inclusion.)

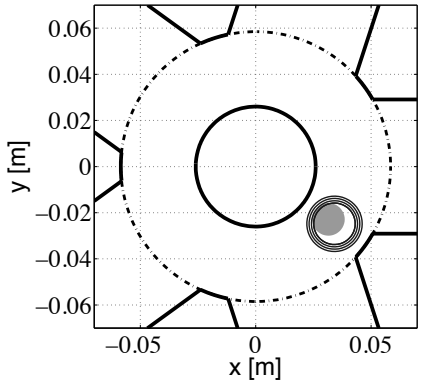

Fig. 8. Geometry and reconstruction for "layer 2": thick solid curves – PEC boundaries; gray circular area – bubble of higher density as compared to the background medium that occupies the remaining portion of the annular region $2.6 \text{ cm} < r < 6.54 \text{ cm}$; and thin solid circles – the five best local optima in the database according to the criterion (6).

TABLE II
THE FIVE BEST LOCAL MINIMA THAT ARE FOUND IN THE DATABASE FOR LAYER 2, WHERE THESE ARE SORTED IN TERMS OF THE VALUE OF THE DEVIATION EQ.(6) WITH THE SMALLEST VALUE ON THE FIRST ROW.

Inclusion					Background	
r_0 [m]	x [m]	y [m]	ϵ_{r} [-]	σ [S/m]	ϵ_{r} [-]	σ [S/m]
0.012	0.0341	-0.0248	4.37	0.067	3.35	0.037
0.010	0.0341	-0.0248	4.88	0.065	3.35	0.037
0.011	0.0341	-0.0248	4.63	0.060	3.35	0.037
0.009	0.0341	-0.0248	5.14	0.059	3.35	0.037
0.009	0.0341	-0.0248	5.14	0.071	3.35	0.037

We conclude that a database can be exploited to predict the background material parameters in the fluidized bed in a robust manner. In addition, information of changes in the granule density, such as bubbles, is feasible to detect. We have tested this on a large number of randomly generated cases with satisfactory results. Here, two representative examples are shown in Fig. 6 and Fig. 8.

V. CONCLUSION

We have described two measurement techniques for closed metal vessels: (i) eigenfrequencies for weakly damped cavities; and (ii) scattering matrix for strongly damped cavities. Also, we presented some comparative results on the estimation of the permittivity of a plexiglas cylinder, where we conclude that the two measurement techniques yield results that are very close to each other. Finally, we demonstrate by means of a computational study that it is feasible to exploit an arrangement with aperture antennas the perform reliable measurements for an inhomogeneous fluidized bed given a database that stores the system response for different process states.

REFERENCES

[1] E. Nyfors and P. Vainikainen, *Industrial Microwave Sensors*. Artech House, 1989.
[2] B. Larsson, B. A. Bengtsson, and M. Gustafsson, "Nondestructive detection of decay in living trees," *Tree Physiology*, vol. 24, no. 7, pp. 853–858, 2004.
[3] K. Harada, Y. Kozima, Y. Fujii, and S. Takeuchi, "Measurements of blast furnace inner-state by magnetometers," *IEEE Trans. Magn.*, vol. MAG-16, no. 5, pp. 698–700, September 1980.
[4] S. Kobayashi and S. Miyahara, "A particulate flow meter using microwaves," in *Proc. IMEKO*, 1985, pp. 112–119.
[5] A. Toropainen, P. Vainikainen, and E. Nyfors, "A microwave humidity sensor for difficult environmental conditions," in *Proc. 17th European Microwave Conference*, 1987, pp. 887–891.
[6] H. Wang, P. Senior, R. Mann, and W. Yang, "Online measurement and control of solids moisture in fluidised bed dryers," *Chemical Engineering Science*, vol. 64, no. 12, pp. 2893 – 2902, 2009.
[7] T. R. McKeen and T. S. Pugsley, "The influence of permittivity models on phantom images obtained from electrical capacitance tomography," *Meas. Sci. Technol.*, vol. 13, no. 12, pp. 1822–1830, 2002.
[8] J. M. Jin, *The Finite Element Method in Electromagnetics (2nd Edition)*. New York, NY: John Wiley & Sons, 2002.
[9] D. M. Pozar, *Microwave engineering*. NY: Wiley, 1998.